PCCP

PAPER

View Article Online
View Journal | View Issue

Cite this: *Phys. Chem. Chem. Phys.*, 2019, **21**, 9785

Shock wave and modelling study of the dissociation pathways of $(C_2F_5)_3N$†

C. J. Cobos,[a] K. Hintzer,[b] L. Sölter,[c] E. Tellbach,[c] A. Thaler[b] and J. Troe *[cd]

Received 26th February 2019,
Accepted 11th April 2019

DOI: 10.1039/c9cp01142k

rsc.li/pccp

The thermal decomposition of perfluorotriethylamine, $(C_2F_5)_3N$, was investigated in shock waves by monitoring the formation of CF_2. Experiments were performed over the temperature range of 1120–1450 K with reactant concentrations between 100 and 1000 ppm of $(C_2F_5)_3N$ in the bath gas Ar and with [Ar] in the range of (0.7–5.5) $\times$ 10^{-5} mol cm^{-3}. The experiments were accompanied by quantum-chemical calculations of the energies of various dissociation paths and by rate calculations, in particular for the dissociation of C_2F_5 *via* $C_2F_5 \rightarrow CF_3 + CF_2$. The overall reaction can proceed in different ways, either by a sequence of successive C–N bond ruptures followed by fast C_2F_5 decompositions, or by a sequence of alternating C–C and C–N bond ruptures. A cross-over between the two pathways can also take place. At temperatures below about 1300 K, yields of less than one CF_2 per $(C_2F_5)_3N$ decomposed were observed. On the other hand, at temperatures around 2000 K, when besides the parent molecule, CF_3 also dissociates, yields of six CF_2 per $(C_2F_5)_3N$ decomposed were measured. The rate-delaying steps of the dissociation mechanism at intermediate temperatures were suggested to be the processes $(C_2F_5)NCF_2 \rightarrow (C_2F_5)N + CF_2$ and $(CF_2)N \rightarrow N + CF_2$. The reduction of the CF_2 yields at low temperatures was tentatively attributed to a branching of the mechanism at the level of $(C_2F_5)_2NCF_2$, from where the cyclic final product perfluoro-*N*-methylpyrrolidine, $(C_4F_8)NCF_3$, is formed which was identified in earlier work from the literature.

1. Introduction

Perfluorotriethylamine, $(C_2F_5)_3N$, has a number of interesting properties. On the one hand, it may serve as a benign liquid reaction medium for Lewis acid-catalyzed organic reactions[1] and other preparative applications. On the other hand, its structure is remarkable, being characterized by a nearly planar C_3N skeleton with CNC angles near to 120°.[2] This skeleton is surrounded by an "inner shell" of CF_2 groups and an "outer shell" of CF_3 groups. The structure of $(C_2F_5)_3N$ has been discussed in relation to that of other fluorinated triamines such as $(CF_3)_3N$,[3] $(CH_2CF_3)_3N$,[4] and $(SF_5)_3N$.[5] Because of its favorable properties, $(C_2F_5)_3N$ has also been considered as an alternative to environmentally more harmful halons.[6] In a study of the thermal decomposition of undiluted gaseous $(C_2F_5)_3N$ in a flow system, by employing gas chromatography (GC) and GC/mass spectrometry (MS) analyses of the final products, perfluoro-*N*-methylpyrrolidine, $(C_4F_8)NCF_3$, was identified.[6] In order to shed more light on the elementary steps of the pyrolysis, shock wave studies of the thermal decomposition of $(C_2F_5)_3N$ diluted in Ar appeared promising. As the decomposition may proceed through different pathways, however, the interpretation of the experiments had to be accompanied by quantum-chemical calculations of the energetics of the reactions involved. That is the subject of the present article.

At sufficiently high temperatures, an overall decomposition

$$(C_2F_5)_3N \rightarrow 3\,C_2F_5 + N \quad \Delta H^\circ_{298} = 905\ \text{kJ mol}^{-1} \qquad (1)$$

(with $\Delta H^\circ_{f,298}(C_2F_5)_3N = -3138$ kJ mol^{-1} from ref. 7, $\Delta H^\circ_{f,298}(C_2F_5) = -901.9$ kJ mol^{-1} and $\Delta H^\circ_{f,298}(N) = 472.7$ kJ mol^{-1} from ref. 8; values for 298 K) would be accompanied by the dissociation of C_2F_5,[9,10]

$$C_2F_5 \rightarrow CF_3 + CF_2 \quad \Delta H^\circ_{298} = 243.8\ \text{kJ mol}^{-1} \qquad (2)$$

which then could be followed by CF_3 dissociation[11,12]

$$CF_3 \rightarrow CF_2 + F \quad \Delta H^\circ_{298} = 355.5\ \text{kJ mol}^{-1} \qquad (3)$$

and, finally, by CF_2 dissociation

$$CF_2 \rightarrow CF + F \quad \Delta H^\circ_{298} = 517.6\ \text{kJ mol}^{-1} \qquad (4)$$

(unless stated differently, enthalpies in this work are from ref. 8).

[a] *INIFTA, Facultad de Ciencias Exactas, Universidad Nacional de La Plata, Argentina*
[b] *Dyneon GmbH, Gendorf, D-84504 Burgkirchen, Germany*
[c] *Institut für Physikalische Chemie, Universität Göttingen, Tammannstr. 6, D-37077 Göttingen, Germany. E-mail: jtroe@gwdg.de*
[d] *Max-Planck-Institut für biophysikalische Chemie, Am Fassberg 11, D-37077 Göttingen, Germany*

† Electronic supplementary information (ESI) available. See DOI: 10.1039/c9cp01142k

In more detail, the dissociation (1) could proceed by a sequence of C–N bond ruptures

$$(C_2F_5)_3N \rightarrow (C_2F_5)_2N + C_2F_5 \quad (5)$$

$$(C_2F_5)_2N \rightarrow (C_2F_5)N + C_2F_5 \quad (6)$$

$$(C_2F_5)N \rightarrow N + C_2F_5 \quad (7)$$

which would be followed by C_2F_5 dissociations (2) (and, at a slower rate, by CF_3 dissociations (3)). Because of the compact structure of $(C_2F_5)_3N$, also a dissociation sequence of alternating C–C and C–N bond ruptures

$$(C_2F_5)_3N \rightarrow (C_2F_5)_2NCF_2 + CF_3 \quad (8)$$

$$(C_2F_5)_2NCF_2 \rightarrow (C_2F_5)_2N + CF_2 \quad (9)$$

$$(C_2F_5)_2N \rightarrow (C_2F_5)NCF_2 + CF_3 \quad (10)$$

$$(C_2F_5)NCF_2 \rightarrow (C_2F_5)N + CF_2 \quad (11)$$

$$(C_2F_5)N \rightarrow (CF_2)N + CF_3 \quad (12)$$

$$(CF_2)N \rightarrow N + CF_2 \quad (13)$$

appears possible. At the level of $(C_2F_5)_2N$ and $(C_2F_5)N$ a cross-over between the C–N and the C–C bond-breaking pathways would be possible.

$(C_2F_5)_3N$ has a low vapour pressure which, nevertheless, allows for the preparation of gaseous reactant/Ar mixtures suitable for shock wave experiments. The progress of the decomposition then can conveniently be followed by recording time-resolved UV absorption signals from CF_2 near 248 nm (see ref. 13 and 14 for high-temperature absorption coefficients of CF_2). Additional observations near 200 nm might be considered for the detection of CF_3.[15] At temperatures where CF_2 becomes unstable, also absorption signals from CF might become observable.[16] By analyzing absorption-time profiles, at first, the CF_2 yields are of relevance. Second, the time dependence of the CF_2 signals would be analyzed with respect to the sequence (5)–(7) followed by reactions (2) and (3) or the sequence (8)–(13) with the possibility of cross-over between the two pathways. Some speculations about the ultimate formation of $(C_4F_8)NCF_3$ in the present work were also made. In high temperature experiments, finally, the kinetics of N/F/CF_2 mixtures of known composition becomes accessible.

In the following, the description of experimental results is preceded by quantum-chemical calculations which facilitate the interpretation of the recorded CF_2 yields and of the time dependence of the recorded concentration profiles of CF_2. As the decomposition of C_2F_5 *via* reaction (2) represents an important intermediate step of the mechanism and as only controversial information on its rate is available,[9,10] a modelling of this rate also appeared desirable.

2. Quantum-chemical calculations of reaction energies

The enthalpies of reactions (2) and (5)–(13) (at 0 K) were determined by using a variety of DFT models, combined with a 6-311+G(3df) basis set, and using the Gaussian set of codes.[17] In detail, B3LYP,[18,19] M06-2X,[20] BMK,[21] and ωB97X-D[22] models were used. The quality of the DFT results was tested for the dissociation of $(C_2F_5)N$ in reactions (7) and (12) by also performing high-level *ab initio* CBS-QB3[23] and G4[24] calculations. As the agreement between the DFT and the *ab initio* calculations for the $(C_2F_5)N$ dissociations appeared satisfactory, only DFT calculations were made for the dissociation of larger species. A comparison of the results obtained by using the various models is given in the ESI.†

ΔH_0^0 values obtained by the ωB97X-D calculations are summarized in Table 1. Except for the dissociation of $(C_2F_5)N \rightarrow CF_2N + CF_3$ where a barrier for the reverse reaction of about 20 kJ mol^{-1} was found, no barriers beyond ΔH_0^o were observed for other reactions of the mechanism. The calculated value of ΔH_0^o = 237 kJ mol^{-1} for the dissociation of C_2F_5 agreed satisfactorily with the literature value[8] of 240.2 kJ mol^{-1}. The resulting overall reaction enthalpy of ΔH_0^o = 939 kJ mol^{-1} for reaction (1) (obtained from Table 1; calculated for 0 K) also appeared consistent with the estimate of ΔH_{298}^o = 905 kJ mol^{-1} as given above (based on ref. 7 and 8 for 298 K). The results of Table 1 are illustrated in Fig. 1. They illustrate possibilities for cross-over between the C–N bond ruptures (5)–(7) accompanied by C_2F_5 dissociation (2) and the pathway of alternating C–C and C–N bond ruptures (8)–(13).

A few pecularities in the sequence of reactions (8)–(13) should be noted: the alternation of high- and low-activation barrier steps in the sequence (8)–(13) indicates ''bottle-necks'' at reactions (11) and (13) which have particularly high barriers. Furthermore, while all other steps in the sequences (5)–(7) and (8)–(13) are of simple bond-fission character, reaction (12) involves a rigid activated complex. At least at intermediate temperatures this reduces the CF_2 yield of the overall reaction. Only at sufficiently high temperatures, when all reactions are fast, one should obtain a yield of six CF_2 per $(C_2F_5)_3N$ decomposed. This prediction could be controlled easily in experiments under conditions where reaction (4) does not consume CF_2.

Apart from the energetics of steps (5)–(7) and (8)–(13), the rate of C_2F_5 decomposition (2) is of importance. We felt that an up-dated modelling of the falloff curves of reaction (2) was necessary.[25,26] This was done with the formalism employed in

Table 1 Reaction enthalpies at 0 K in kJ mol^{-1} (obtained by calculations using the ωB97X-D model;[22] results from other models are summarized in the ESI)

Reaction		ΔH_0^o
$(C_2F_5)_3N \rightarrow (C_2F_5)_2N + C_2F_5$	(5)	327.2
$(C_2F_5)_2N \rightarrow (C_2F_5)N + C_2F_5$	(6)	320.9
$(C_2F_5)N \rightarrow N + C_2F_5$	(7)	291.2
$C_2F_5 \rightarrow CF_3 + CF_2$	(2)	237.2
$(C_2F_5)_3N \rightarrow (C_2F_5)_2NCF_2 + CF_3$	(8)	345.6
$(C_2F_5)_2NCF_2 \rightarrow (C_2F_5)_2N + CF_2$	(9)	218.0
$(C_2F_5)_2N \rightarrow (C_2F_5)NCF_2 + CF_3$	(10)	46.0
$(C_2F_5)NCF_2 \rightarrow (C_2F_5)N + CF_2$	(11)	512.5
$(C_2F_5)N \rightarrow CF_2N + CF_3$	(12)	103.8
(TS12)		123.4
$CF_2N \rightarrow N + CF_2$	(13)	423.5

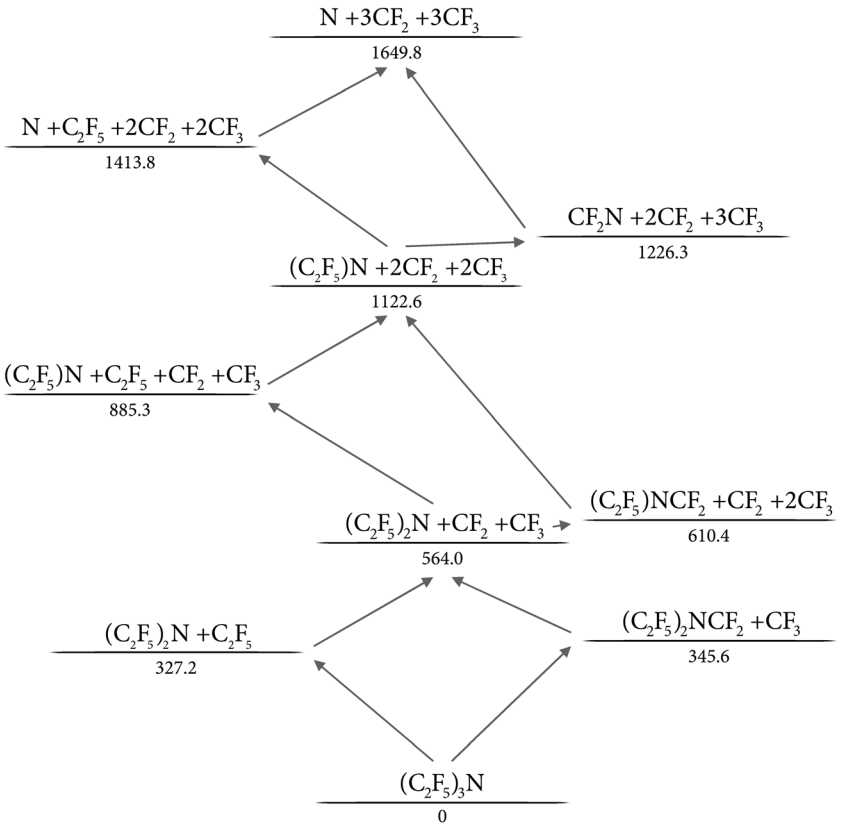

Fig. 1 Energetics of dissociation pathways (reaction enthalpies at 0 K in kJ mol^{-1} obtained by ωB97X-D calculations of the present work, see the text and the ESI†).

our earlier work (see, *e.g.* ref. 13, 15 and 16; for more details, see the ESI†). The results are shown in Fig. 2. The calculation of individual rate constants for other reaction steps of the pathway was beyond the scope of the present work. Likewise, the complex rearrangement processes leading to the final cyclic product $(C_4F_8)NCF_3$ were not further investigated here.

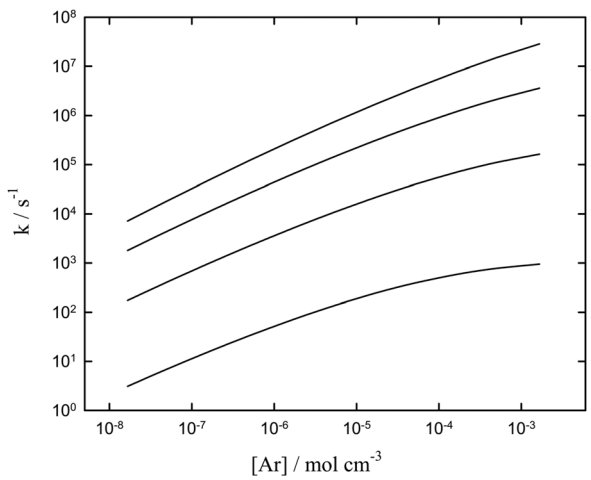

Fig. 2 Modelled falloff curves for the dissociation $C_2F_5 \rightarrow CF_2 + CF_3$ (2) (pseudo-first order rate constans *k*; for details of the calculations, see the ESI†; *T* = 1000, 1250, 1500, and 1750 K, from bottom to top).

3. Experimental technique and results

Our shock wave technique has been described before (for details, see, *e.g.* ref. 12–16). Mixtures of $(C_2F_5)_3N$ (from Fluorochem, purity 96%) and Ar (from Air Liquide, purity 99.9999%) were prepared in mixing vessels outside the shock tube and then introduced into the tube. Usually, low-concentration mixtures of about 200 ppm of $(C_2F_5)_3N$ in Ar were used, but higher concentrations (up to about 1000 ppm $(C_2F_5)_3N$) were also employed. The experimental conditions behind incident and reflected shock waves are included in Table 2 (and given in the figure captions). UV absorption signals were recorded at selected wavelengths over the range of 200–280 nm. The majority of the experiments were conducted at 248 nm where CF_2 absorbs most strongly (CF_2 absorption coefficients from eqn (5) of ref. 13 were used for the determination of absolute CF_2 yields during $(C_2F_5)_3N$ decomposition).

The recorded absorption-time profiles showed a number of interesting properties. Fig. 3 gives an example. The Schlieren peak at time zero indicates the arrival of the incident shock at the observation window. At the corresponding temperature of 1371 K, the concentration of CF_2 increases up to a yield of $Y(CF_2) = [CF_2]/[(C_2F_5)_3N]_{t=0} = 1$. Closer inspection of the signal near time zero indicates no absorption from the parent molecule. The nature of the absorbing species CF_2 could uniquely be identified by the wavelength dependence of the signal. At the

Table 2 Apparent rate constants k of eqn (16), k_{in} of eqn (19), and CF_2 yields Y. (a) Experiments with $Y = 1$ and $k_{in} \approx k$; (b) experiments with $Y < 1$ and $k_{in} \approx k$; (c) experiments with $Y < 1$ and $k > k_{in}$; see the text

T/K	[Ar]/10^{-5} mol cm^{-3}	k/s^{-1}	k_{in}/s^{-1}	Y
(a)				
1451	4.1	1.4×10^5		
1430	2.7	6.3×10^4		
1371	0.71	2.6×10^4		
1367	4.3	3.4×10^4		
1347	4.3	3.6×10^4		
1320	2.2	1.8×10^4		
1297	0.76	1.1×10^4		
(b)				
1296	4.5	7.8×10^3		0.85
1246	4.8	4.9×10^3		0.53
1226	5.0	3.2×10^3		0.43
1211	4.9	2.8×10^3		0.39
1160	5.4	1.5×10^3		0.14
1133	5.5	1.1×10^3		0.09
1130	5.3	9.0×10^2		0.08
(c)				
1246	4.8		1.8×10^3	
1226	5.0		1.0×10^3	
1196	5.3		1.2×10^2	
1159	5.4		1.7×10^2	
1132	5.3		6.3×10^1	
1122	5.2		3.3×10^1	

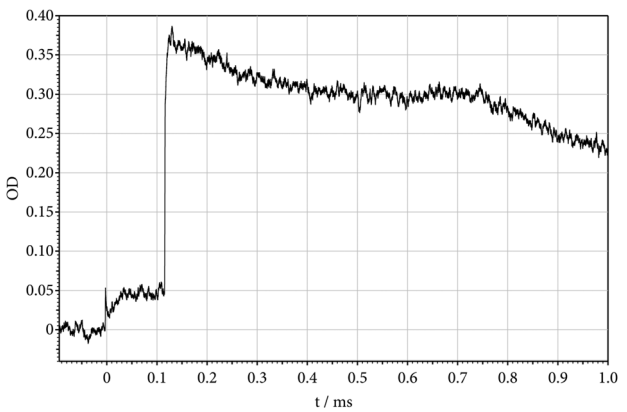

Fig. 3 Decomposition of $(C_2F_5)_3N$ behind the incident shock wave (absorption-time profile of formed CF_2 at 248 nm; incident shock: T = 1371 K, [Ar] = 7.1 × 10^{-6} mol cm^{-3}; reflected shock: T = 2818 K, [Ar] = 1.6 × 10^{-5} mol cm^{-3}; 212 ppm $(C_2F_5)_3N$ in Ar; OD = $\varepsilon \cdot [CF_2] \cdot l$ with l = 9.4 cm and ε = 3.6 × 10^6 cm^2 mol^{-1} for 1371 K and ε = 1.8 × 10^6 cm^2 mol^{-1} for 2818 K; instantaneous dissociation of CF_3 at the time of arrival of the reflected shock, followed by the slower dissociation (4) of CF_2 with k = 103 s^{-1} and secondary reactions, see the text).

time of arrival of the reflected shock (at T = 2818 K), the absorption rises abruptly to a level corresponding to $Y(CF_2) = 6$. This value of $Y = 6$ corresponds to a completion of reaction (1) followed by reactions (2)–(4) within less than 2 μs (the halflife of C_2F_5 here is about 0.025 μs, see Fig. 2, and the halflife of CF_3 is about 1.8 μs, see ref. 12). The decrease in the absorption signal behind the reflected wave, on the one hand, reflects the dissociation of CF_2 (halflife of about 700 μs, see ref. 12). On the other hand, there is evidence for a superimposed absorption which seems to arise from a species which has an even larger absorption coefficient than CF_2. Tentatively we attribute this additional absorption to CF, being formed by the dissociation of CF_2 in reaction (4) and/or a reaction

$$N + CF_2 \rightarrow NF + CF \quad \Delta H^\circ_{298} = 198.5 \text{ kJ mol}^{-1} \qquad (14)$$

As information on further reactions like

$$NF + M \rightarrow N + F + M \quad \Delta H^\circ_{298} = 319.1 \text{ kJ mol}^{-1} \qquad (15)$$

(M denotes the bath gas) and reactions of $(CF_2)N$ is not available, an investigation of the superimposed absorption "humps" shown in Fig. 3 did not appear warranted at the present time. Because the additional absorptions appeared only at temperatures above 2000 K, our study of $(C_2F_5)_3N$ dissociation was not perturbed by this complication. The assumption of the presence of CF, however, did not appear improbable, because its absorption coefficient at 248 nm in ref. 16 was found to be about 3 times that of CF_2.

The formation of CF_2 was studied behind incident and reflected shock waves, as shown in Fig. 3 and 4. The temperature of the latter experiment (1347 K) and the rate of formation of CF_2 (accounting for the compressed time scale, behind the incident wave) were close to that of Fig. 3, while the bath gas concentrations differed markedly ([Ar] = 7.1 × 10^{-6} mol cm^{-3} behind the incident shock as shown in Fig. 3 and [Ar] = 4.2 × 10^{-5} mol cm^{-3} behind the reflected shock as shown in Fig. 4). A pressure effect thus was not observed. The CF_2 yields in both cases reached $Y \approx 1$. This changed at lower temperatures. The CF_2 concentration at 1246 K, as shown in Fig. 5, rose up to a yield of $Y \approx 0.6$ only. As Fig. 4 and 5 were obtained with the same reaction mixture (209 ppm of $(C_2F_5)_3N$ in Ar), this observation could not have been produced by concentration uncertainties (with reaction mixtures above 1000 ppm, the small $(C_2F_5)_3N$ vapour pressure caused problems with accurate concentration determinations). Because of the limitation of the observation time behind the reflected shock to about 1 ms, the drop of Y with decreasing temperature could only be followed down to about $T \approx 1130$ K.

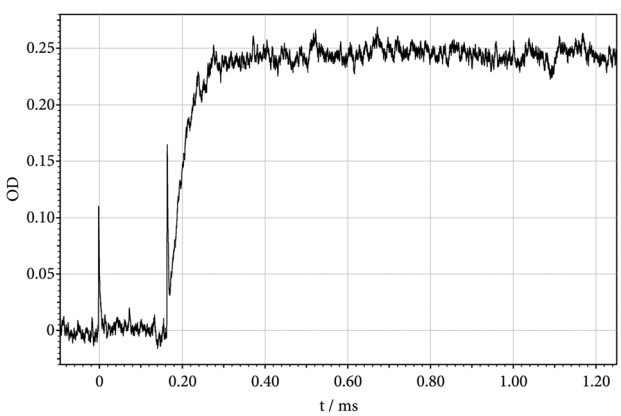

Fig. 4 Decomposition of $(C_2F_5)_3N$ behind the reflected shock wave (absorption-time profile of formed CF_2 at 248 nm; T = 1347 K, [Ar] = 4.2 × 10^{-5} mol cm^{-3}; 209 ppm $(C_2F_5)_3N$ in Ar).

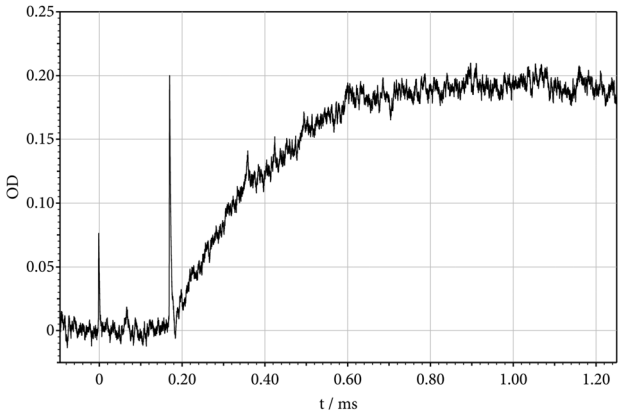

Fig. 5 The same as Fig. 4, but at lower temperature (T = 1246 K, [Ar] = 4.8×10^{-5} mol cm^{-3}; 209 ppm $(C_2F_5)_3N$ in Ar; ε(1246 K)/ε(1347 K) ≈ 1.15[13]).

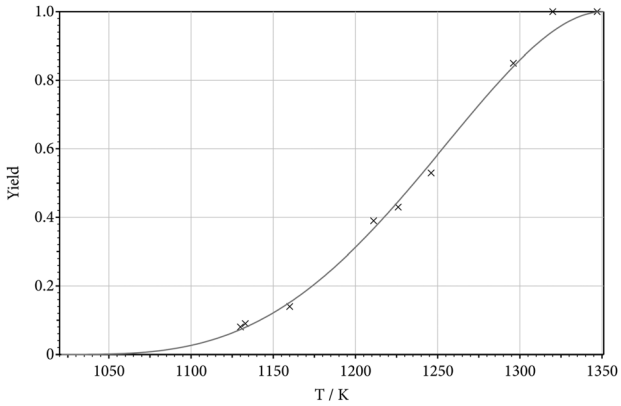

Fig. 7 Apparent final CF_2 yields $Y = [CF_2]/[(C_2F_5)_3N]_{t=0}$ over the range of 1130–1450 K (representation by eqn (18)).

The recorded absorption-time profiles of CF_2 were evaluated in two different ways. For the temperature range of 1130–1540 K, where a practically time-independent final CF_2 yield $Y(T)$ was reached within the observation time, an effective rate law

$$[CF_2]_t/[(C_2F_5)_3N]_{t=0} \approx Y(T)\{1 - \exp(-k(T)t)\} \quad (16)$$

appeared suitable. The resulting rate constants $k(T)$ and yields $Y(T)$ are summarized in Table 2 and plotted in Fig. 6 and 7, respectively. The Arrhenius representation of $k(T)$ as shown in Fig. 6 led to

$$k(T) \approx 2.5 \times 10^{13} \exp(-213 \text{ kJ mol}^{-1}/RT)\text{s}^{-1} \quad (17)$$

while $Y(T)$ in the form of ref. 27 was approximated by

$$Y(T) \approx [1 - (T - T_e)/(T_e - T_m)][(T - T_0)/(T_e - T_0)]^{(T_e - T_0)/(T_e - T_m)} \quad (18)$$

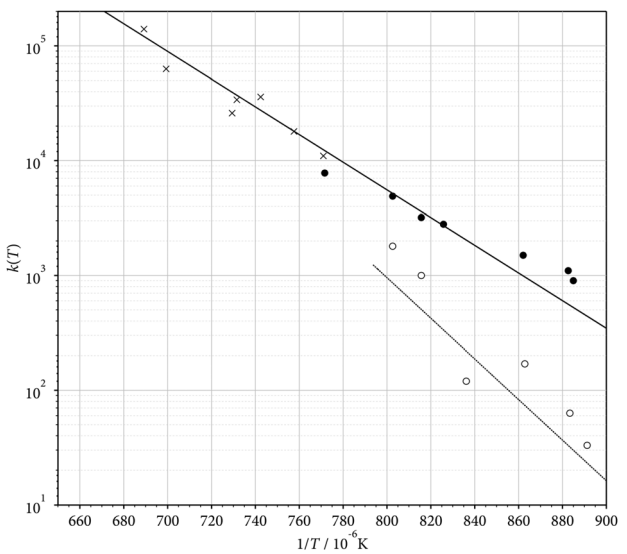

Fig. 6 Apparent rate constants k of eqn (17) and k_{in} of eqn (20) (×: see Table 2a); (●: see Table 2b); (○: see Table 2c); k represented by eqn (17) with the points × and ●; k_{in} represented by eqn (20) with the high-temperature limit of k and points (○; see the text).

with the parameters T_e = 1351 K, T_0 = 1020 K, and fitted T_m = 1295 K. Alternatively, the formation of CF_2 was characterized by its initial rate

$$\left.\frac{d[CF_2]}{dt}\right|_{t=0} \approx k_{in}(T)\left[(C_2F_5)_3N\right]_{t=0} \quad (19)$$

Values of $k_{in}(T)$ could also be derived for lower temperatures where a final stationary CF_2 level could not be attained within the observation time. Fig. 6 and Table 2 include values of $k_{in}(T)$. In Arrhenius form they are represented by

$$k_{in}(T) \approx 1.4 \times 10^{17} \exp(-339 \text{ kJ mol}^{-1}/RT)\text{s}^{-1} \quad (20)$$

when high-temperature limiting values of $k(T)$ near 1500 K are combined with the measured points of k_{in} over the range of 1130–1250 K (one should note that the scatter of the values of k_{in} is due to some uncertainties of the $(C_2F_5)_3N$ concentration in the reaction mixtures, see eqn (19); this problem does not exist for the measurements of $k(T)$; thus eqn (20) is of qualitative importance only). The relation of the apparent $k(T)$, $k_{in}(T)$, and $Y(T)$ to the dissociation pathways illustrated in Fig. 1 will be considered in Section 4.

It should be noted that experiments at higher temperatures (see Fig. 8), correspond to the dissociation of CF_3 through reaction (3). The increase of the CF_2 absorption behind the absorption step at the time of arrival of the reflected shock wave as shown in Fig. 8 (T = 1854 K) leads to a value of the rate constant for reaction (3) of $k_3 \approx 3.5 \times 10^3$ s^{-1}. This is in perfect agreement with the result obtained from the CF_3 dissociation study of ref. 12. While this confirms the overall mechanism, it limits the study of the later stages of $(C_2F_5)_3N$ dissociation. One observes that the absorption step at the time of arrival of the reflected wave as shown in Fig. 8 corresponds to $Y \approx 2$ while finally $Y \approx 3$ is reached (as most clearly seen in the inset of Fig. 8). Apparently, CF_3 dissociation and the slower steps of the $(C_2F_5)_3N$ dissociation here are superimposed and could not be separated in the present experiments. Monitoring CF_3 near 200 nm did not help, as the strong CF_2 absorption at high temperatures extends from 248 nm down to 200 nm and is

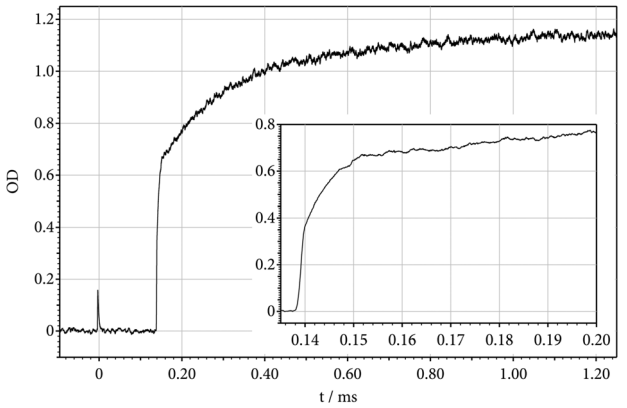

Fig. 8 CF_2 formation by the decomposition of CF_3 produced during the decomposition of $(C_2F_5)_3N$ (reflected shock wave at 1854 K and [Ar] = 2.9×10^{-5} mol cm^{-3}; $[(C_2F_5)_3N]_{t=0}$/[Ar]= 528 ppm; the inset resolves CF_2 formation during the late stages of $(C_2F_5)_3N$ decomposition; for details see the text).

then superimposed on the CF_3 absorption. In any case, in the intermediate temperature range between 1500 and 2000 K a CF_2 yield of $Y = 6$ was not reached. On the other hand, Y approached unity in the range of 1300–1500 K.

4. Discussion

Although only limited experimental and theoretical information about the reaction network of Fig. 1 became available, a number of important conclusions could be drawn. The following pathways appear possible: (i) $(C_2F_5)_3N$ dissociates in a sequence of C–N bond ruptures (5)–(7) followed by fast dissociation (2) of the product C_2F_5; (ii) $(C_2F_5)_3N$ dissociates in a sequence of C–C bond ruptures (8), (10), and (12), followed by C–N bond ruptures (9), (11), and (13); (iii) two pathways (i) and (ii) occur in parallel with the possibility of cross-over at the stages of formation of $(C_2F_5)_2N$ and $(C_2F_5)N$. At temperatures where the reactions of pathways (i)–(iii) are complete, and where CF_3 dissociates through reaction (3) while reaction (4) is too slow to consume CF_2, the overall CF_2 yield $Y(T)$ should be 6. This was indeed observed, but this does not allow one to distinguish between the pathways.

An exclusive mechanism (i) can be excluded for a number of reasons: although the enthalpies of the reaction steps slightly decrease from (5) to (7), rate constants k_5, k_6, and k_7 should be of similar magnitude. With a fast dissociation of C_2F_5 this would then result in $Y = 3$. A modelling of the kinetics indicates that the effective rate constant $k(T)$ in eqn (16) would correspond to about $k(T) \approx 2\ k_5$. Furthermore, the derived value of $k(T)$ should correspond to a simple bond fission process with a preexponential factor of the order of 10^{15}–10^{17} s^{-1} while the activation energy should be of the order of the reaction enthalpy of reaction (5). These expectations are in disagreement with the experimental observations from Section 3.

Mechanism (ii) would have properties which are in closer agreement with the experiments. Particularly in its later stages, this mechanism would be governed by the alternation of low and high reaction barriers such that the reaction flux may "get stuck" at the level of $(C_2F_5)N + 2CF_3 + CF_2$. This would explain CF_2 yields $Y(T)$ near unity for experiments in the range of 1100–1500 K. However, the apparent rate constant k should again correspond to a simple bond fission and $Y(T)$ should be close to unity even at the lowest temperatures of the present experiments. The latter two expectations are again in disagreement with the experimental observation.

It remains to inspect mechanism (iii) with the possibility of at least a partial cross-over between the two pathways (i) and (ii). The observation of a CF_2 yield near unity over a wide temperature range suggests that the reaction gets stuck at the level of $(C_2F_5)NCF_2 + CF_2 + 2\ CF_3$, regardless of whether pathway (ii) or (i) with a cross-over at the level of $(C_2F_5)_2N$ precedes the approach of the bottle-neck of reaction (10). Unfortunately, CF_2 formation beyond the bottle-neck at higher temperatures in our experiments could not be distinguished from CF_2 formation by decomposition of CF_3 (see Section 3). However all evidence is for a slow completion of the reaction after reaching the bottle-neck. Finally, the properties of the apparent rate constant $k(T)$, $k_{in}(T)$, and the decrease of $Y(T)$ to values below unity at low temperatures need to be rationalized. While the Arrhenius representation of $k(T)$ by eqn (17) corresponds more to a rigid-activated complex process, $k_{in}(T)$ in eqn (19) would appear consistent with a loose-activated complex of bond-fission type, like that expected for k_5 and/or k_8 (from reactions (5) and (8)).

It appears more difficult to explain the decrease of $Y(T)$ with decreasing temperature, while $k_{in}(T)$ corresponds to k_5 and/or k_8. An answer may come from speculations about the formation of the low-temperature final product $(C_4F_8)NCF_3$. If there is a branching of the reaction flux at the level of $(C_2F_5)_2NCF_2$, *i.e.* beyond the low-temperature rate-determining step (8) of pathway (ii), then the rate constant $k_{in}(T)$ for CF_2 formation would not be influenced while the CF_2 yield would be. This branching by as yet unidentified rearrangement processes should involve rigid activated complexes with lower preexponential factors and activation energies than the competing bond fission (9). It would then win at lower temperatures and reduce here the CF_2 yield of $Y(T)$, and this was observed in our experiments. Obviously, more work would be necessary to validate the given interpretation which would be able to reconcile the present high-temperature observations with the earlier low-temperature measurements of final products from ref. 6.

5. Conclusions

The combination of quantum-chemical calculations and experiments monitoring the formation of product CF_2 in $(C_2F_5)_3N$ decomposition provided evidence for a sequence of C–N and C–C bond ruptures taking place simultaneously. Apparently, dissociation steps in the inner CF_2-shell and in the outer CF_3-shell occur in parallel and proceed as simple bond fission processes. The alternation of bond energies for the C–C and C–N bond rupture sequence of reactions (8)–(13) deserves particular attention. At temperatures that are sufficiently high for reactions (5)–(13) to occur,

but low enough to keep CF_2 undissociated, the observed overall yield of 6 CF_2 per consumed $(C_2F_5)_3N$ confirms the kinetic analysis.

Details of the mechanism would not have been understood without the quantum-chemical calculations. As the decomposition of C_2F_5 through reaction (2) forms an essential part of the mechanism and its rate was not well known before, the falloff curves of this important reaction also had to be modelled. Finally, the present experiments at temperatures above about 2000 K generate mixtures of N, F, and CF_2 in a concentration ratio 1 : 3 : 6. Recording absorption-time profiles for this mixture suggests contributions from CF_2 and CF, the latter not only arising from CF_2 dissociation (4) but also from other, so far unidentified processes.

Finally, a branching of the mechanism at the level of $(C_2F_5)_2NCF_2$, on the one hand, may provide an explanation for the low-temperature production of an end product like perfluoro-*N*-methylpyrrolidene, $(C_4F_8)NCF_3$, such as was observed earlier in ref. 6; on the other hand, this detail may also be responsible for the properties of the CF_2 yields observed at the low-temperature end of the present experiments.

Conflicts of interest

There are no conflicts to declare.

Acknowledgements

Financial support from the Deutsche Forschungsgemeinschaft (Projekt TR69-20-3) is gratefully acknowledged. Open Access funding provided by the Max Planck Society.

References

1 H. Nakano and T. Kitazume, Organic Reactions Without an Organic Medium, Utilization of Perfluorotriethylamine as a Reaction Medium, *Green Chem.*, 1999, **1**, 21–22.
2 M. Gaensslen, U. Gross, H. Oberhammer and S. Rüdiger, Perfluorotriethylamine: An Amine with Unusual Structure and Reactivity, *Angew. Chem., Int. Ed. Engl.*, 1992, **31**, 1467–1468.
3 H. Bürger, H. Niepel, G. Pawelke and H. Oberhammer, Vibrational Spectra and Normal Coordinate Analysis of CF_3 Compounds: Part XXVII. Perfluorotrimethylamine. Reinvestigation of the Molecular Structure by Electron Diffraction, *J. Mol. Struct.*, 1979, **54**, 159–174.
4 A. Dimitrov, H.-G. Mack, S. Rüdiger, K. Seppelt and H. Oberhammer, Structure and Conformation of Tris(2,2,2-trifluoroethyl)amine, $N(CH_2CF_3)_3$, in the Gaseous and Solid State, *J. Phys. Chem.*, 1994, **98**, 11401–11405.
5 J. B. Nielsen, P. Zylka, M. Kronberg, X. Zeng, K. D. Robinson, S. G. Bott, H. Zhang, J. L. Atwood, H. Oberhammer, H. Willner and J. S. Thrasher, Solid- and Gas-Phase Structures and Spectroscopic and Chemical Properties of Tris(pentafluorosulfanyl)-amine, $N(SF_5)_3$ and Bis(pentafluorosulfanyl)aminyl Radical, $^{\bullet}N(SF_5)_2$, *J. Mol. Struct.*, 2017, **1132**, 11–19.
6 T. Yamamoto, A. Yasuhara, F. Shiraishi, K. Kaya and T. Abe, Thermal Decomposition of Halon Alternatives, *Chemosphere*, 1997, **35**(3), 643–654.
7 V. P. Kolesov and M. P. Kozina, Thermochemistry of Organic and Organohalogen Compounds, *Russ. Chem. Rev.*, 1986, **55**, 912–928.
8 E. Goos, A. Burcat and B. Ruscic, Extended Third Millenium Ideal Gas and Condensed Phase Thermochemical Data Base for Combustion with Updates from Active Thermochemical Tables <ftp.technion.ac.il/pub/supported/aetdd/thermodynamics> Jan 2015.
9 K. Li, E. M. Kennedy and B. Z. Dlogogorski, Experimental and Computational Studies of the Pyrolysis of $CBrF_3$, and the Reaction of $CBrF_3$ with CH_4, *Chem. Eng. Sci.*, 2000, **55**, 4067–4078.
10 A. F. Ainagos, Mechanism and Kinetics of Pyrolysis of Perfluorohexane, *Kinet. Catal.*, 1991, **32**, 720–725.
11 N. K. Srinivasan, M.-C. Su, J. V. Michael, A. W. Jasper, S. J. Klippenstein and L. B. Harding, Thermal Decomposition of CF_3 and the Reaction of $CF_2 + OH \rightarrow CF_2O + H$, *J. Phys. Chem. A*, 2008, **112**, 31–37.
12 C. J. Cobos, A. E. Croce, K. Luther and J. Troe, Shock Wave Study of the Thermal Decomposition of CF_3 and CF_2 Radicals, *J. Phys. Chem. A*, 2010, **114**, 4755–4761.
13 C. J. Cobos, A. E. Croce, K. Luther, L. Sölter, E. Tellbach and J. Troe, Experimental and Modeling Study of the Reaction C_2F_4 (+M) $\leftrightarrow$ $CF_2 + CF_2$ (+M), *J. Phys. Chem. A*, 2013, **117**, 11420–11429.
14 C. J. Cobos, G. Knight, L. Sölter, E. Tellbach and J. Troe, Kinetic and Spectroscopic Studies of the Reaction of CF_2 with H_2 in Shock Waves, *J. Phys. Chem. A*, 2017, **121**, 7827–7834.
15 K. Glänzer, M. Maier and J. Troe, Shock-Wave Study of the High-Temperature UV Absorption and the Recombination of Trifluoromethyl Radicals, *J. Phys. Chem.*, 1980, **84**, 1681–1686.
16 C. J. Cobos, G. Knight, L. Sölter, E. Tellbach and J. Troe, Experimental and Modeling Study of the Multichannel Thermal Dissociation of CH_3F and CH_2F, *Phys. Chem. Chem. Phys.*, 2018, **20**, 2627–2636.
17 M. J. Frisch, *et al.*, *Revision A.02*, Gaussian Inc., Wallingford, CT, USA, 2009.
18 A. D. Becke, Densitiy-Functional Exchange-Energy Approximation with Correct Asymptotic Behavior, *Phys. Rev. A: At., Mol., Opt. Phys.*, 1988, **38**, 3098–3100.
19 C. Lee, W. Yang and R. G. Parr, Development of the Colle-Salvetti Correlation-Energy Formula into a Functional of the Electron Density, *Phys. Rev. B: Condens. Matter Mater. Phys.*, 1988, **37**, 785–789.
20 Y. Zhao and D. G. Truhlar, The M06 Suite of Density Functionals for Main Group Thermochemistry, Thermochemical Kinetics, Noncovalent Interactions, Excited States, and Transition Elements: Two New Functionals and Systematic Testing of Four M06-Class Functionals and 12 Other Functionals, *Theor. Chem. Acc.*, 2008, **120**, 215–241.
21 A. D. Boese and J. M. Martin, Development of Density Functionals for Thermochemical Kinetics, *J. Chem. Phys.*, 2004, **121**, 3405–3416.

22 J.-D. Chai and M. Head-Gordon, Long-Range Corrected Hybrid Density Functionals with Damped Atom-Atom Dispersion Corrections, *Phys. Chem. Chem. Phys.*, 2008, **10**, 6615–6620.
23 J. A. Montgomery, M. J. Frisch, J. W. Ochterski and G. A. Petersson, A Complete Basis Set Model Chemistry. VI. Use of Density Functional Geometries and Frequencies, *J. Chem. Phys.*, 1999, **110**, 2822–2827.
24 L. A. Curtiss, P. C. Redfern and K. Raghavachari, Gaussian-4 Theory, *J. Chem. Phys.*, 2007, **126**, 084108.
25 NIST Kinetics Database 17, Version 7.0 (Web Version), Release 1.6.8, Data Version 2015.09.
26 Y. Li, X. Zhang, S. Xiao, Q. Chen, J. Tang, D. Chen and D. Wang, Decomposition Properties of C_4F_7N/N_2 Gas Mixture: An Environmentally Friendly Gas to Replace SF_6, *Ind. Eng. Chem. Res.*, 2018, **57**, 5173–5182.
27 X. Yin, J. Goudriaan, E. A. Latinga, J. Vos and H. J. Spiertz, A Flexible Sigmoid Function of Determinate Growth, *Ann. Bot.*, 2003, **91**, 361–371.